RESONANCE PRODUCTION OF EXCITED u QUARK AT FCC-BASED γp COLLIDERS *

Yusuf Oguzhan Günaydin

Department of Physics, Kahramanmaras Sutcu Imam University
Kahramanmaras, Turkey

Mehmet Sahin

Department of Physics, Usak University, Usak, Turkey

Saleh Sultansoy

TOBB University of Economics and Technology, Ankara, Turkey
and
ANAS Institute of Physics, Baku, Azerbaijan

(Received January 24, 2018; accepted July 19, 2018)

Several Beyond the Standard Model theories proposed that fermions might have composite substructure. The existence of excited quarks is going to be the noticeable proof for the compositeness of Standard Model fermions. For this reason, excited quarks have been investigated by phenomenological and experimental high-energy physicists at various collider options for the last few decades. The Future Circular Collider (FCC) has been recently planned as particle accelerator to be established at CERN. Beside the $\sqrt{s} = 100$ TeV proton–proton collisions, the FCC includes electron–positron and electron–proton collision options. Construction of linear e^-e^+ colliders (or dedicated e-linac) tangential to the FCC will afford an opportunity to handle multi-TeV ep and γp collisions. In this respect, we executed a simulation of the resonance production of the excited u quark at the FCC-based γp colliders with choosing both the polarized and unpolarized photon beams. The findings revealed that the chirality structure of the q^*–q–γ vertex can be determined by the photon beam polarization. The attainable mass limits of the excited u quark reached the highest values when the polarized photon beam was chosen. In addition, the ultimate compositeness scale values can be handled by appropriate choice of the photon beam polarization.

DOI:10.5506/APhysPolB.49.1763

1. Introduction

The Standard Model (SM), the most reliable theory in particle physics, shows incredible consistency with experiments and reaches its last prediction after the CMS and the ATLAS collaborations, which both declared the detection of the Higgs boson [1, 2] in 2012. Despite the marvelous success of the SM on a wide range of phenomena in particle physics, there remain unsolved mysteries that the SM does not explain. The quark–lepton symmetry, family replication, charge quantization, plenty numbers of elementary particles, parameters and the likes are unsolved issues in the SM frame. Therefore, numerous models are proposed in an attempt to answer the afore-mentioned problems. One of these approaches, namely, compositeness has an assumption that SM fermions are compound states of more fundamental particles, preons [3, 4]. Numerous preonic models have been suggested by particle physicists for more than forty years [5–14]. Due to preonic interactions caused by preon models, plenty of new types of particles are expected, such as excited quarks and leptons, leptoquarks, leptogluons, diquarks, color sextet quarks, dileptons and so on.

Excited fermions are comprised of excited quarks (q^*) and leptons (l^*) that can be considered as the excited state of SM fermions. They could have spin-1/2 and spin-3/2 states and their masses are expected to be much heavier than SM fermions. As a result, the discovery of excited fermions will be a direct proof of SM quarks' and leptons' compositeness. After the first publication about excited leptons which was written in 1965 [15], scores of theoretical, phenomenological [16–34] and experimental [35–47] researchers have been focused on proving the existence of excited fermions. The historical development of fundamental blocks of the matter [48] shows that new substructures of elementary particles are discovered by new experimental findings and this evidence attracts attention of particle physicists to do research on excited quarks and leptons.

Excited quarks decay into four final states with light jets of ($q^* \to jj$), ($q^* \to j\gamma$), ($q^* \to jW$), and ($q^* \to jZ$). The most recent experimental results regarding excited quark mass are provided by the CMS and ATLAS collaborations [41–47, 49]. q^* mass exclusion limits are $m_{q^*} = 6.0$ TeV for $q^* \to jj$, $m_{q^*} = 5.5$ TeV for $q^* \to j\gamma$, $m_{q^*} = 3.2$ TeV for $q^* \to jW$ and $m_{q^*} = 2.9$ TeV for $q^* \to jZ$. For these experimental limits on excited quark mass, compositeness scale (Λ) is considered to be equal to m_{q^*}.

In this paper, we investigate resonant production of the up-type excited quark (u^*) with dijet final state at two different center-of-mass (CM) energies [50] of the Future Circular Collider (FCC)-based [51] γp colliders [52]. In addition, we neglect possible contact interactions at this stage. We present the FCC-based colliders options and their parameters, specifically γp colliders in Section 2, q^* effective interaction Lagrangian and decay width in

Section 3 and leading order production cross sections and signal-background analysis using unpolarized and polarized photons in Section 4. Finally, outcomes of the u^* mass limitations, the compositeness scale (Λ) inquiries and interpretation of our findings are presented in the last section.

2. FCC-based γp colliders

Throughout the last 40 years of the particle accelerator development, several groups and collaborations proposed linac-ring-type colliders (see reviews [53–59]). Concerning energy frontier lepton–hadron options, VLEPP+UNK, THERA and LHeC were proposed in the 1980s, 1990s and 2000s, respectively. The latter option [60] is planned to be established at CERN around the 2020s. Furthermore, after the Large Hadron Collider (LHC) physics program is completed, the FCC [61] will be seen as experimental particle physics frontier machine by the high-energy physics community. The FCC is planned to have nearly 4 times bigger circumference (Fig. 1) and about 7 times higher center-of-mass energy than the LHC. The FCC is con-

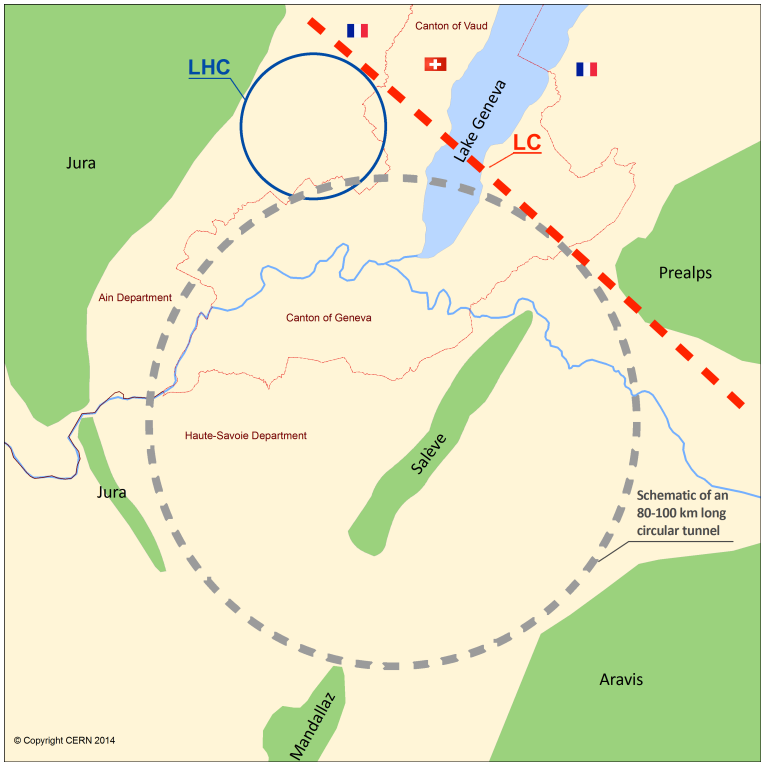

Fig. 1. Schematic drawing of the Future Circular Collider and the Linear Collider.

sidered as three options: (1) the electron–positron (FCC-ee) [62], (2) the proton–proton (FCC-pp) [63] and (3) the electron–proton (FCC-ep) [61] colliders. To measure new findings with high precision, FCC-ee is an appropriate option, notwithstanding, FCC-pp and FCC-ep are needed for deep investigation of interactions. That is, many features of the Higgs boson can be measured by FCC-ee whose collision energy varies between 91 and 350 GeV. However, further measurements such as Higgs self-interactions and top-quark Higgs bosons interaction could be achieved by FCC-pp at 100 TeV center-of-mass energy. Besides, quark substructure discovery might happen at the FCC-ep collider.

With respect to excited quark, we focused on the FCC-based γp collider within the scope of this study. There are several options for lepton–hadron collision but we preferred the FCC-based electron–proton colliders by using International Linear Collider (ILC) and Plasma Wakefield Accelerator-Linear Collider (PWFA-LC) [50]. In addition to the FCC-based *ep* colliders, γp colliders [52, 64] could be utilized by exploiting the Compton backscattering [65–67]. Main parameters of the *ep* and γp colliders which we used in our calculations are listed in Table I.

TABLE I

Energy and luminosity parameters of the ILC⊗FCC- and PWFA-LC⊗FCC-based *ep* and γp colliders.

Collider name	E_e [TeV]	$E_\gamma^{\max}$ [TeV]	$\sqrt{s}_{ep}$ [TeV]	$\sqrt{s}_{\gamma p}^{\max}$ [TeV]	$\mathcal{L}_{\text{int}}$ [fb^{-1}/year]
ILC⊗FCC	0.5	0.42	10	9.1	10–100
PWFA-LC⊗FCC	5	4.15	31.6	28.8	1–10

3. Spin-1/2 excited quark interaction Lagrangian and decay width

Interaction between spin-1/2 excited quarks, SM quarks and gauge bosons is described by the magnetic-type effective Lagrangian [17, 19, 22, 49]

$$L_{\text{eff}} = \frac{1}{2\Lambda}\bar{q^*}\sigma^{\mu\nu}\left[g_s f_s \frac{\lambda_a}{2}F^a_{\mu\nu} + gf\frac{\vec{\tau}}{2}\vec{W}_{\mu\nu} + g'f'\frac{Y}{2}B_{\mu\nu}\right] \times \left(\eta_{\text{L}}\frac{1-\gamma_5}{2} + \eta_{\text{R}}\frac{1+\gamma_5}{2}\right)q + \text{h.c.} \quad (1)$$

As illustrated above, Λ denotes compositeness scale, q^* and q represent spin-1/2 excited quark and ground state quark, respectively, $F^a_{\mu\nu}$, $\vec{W}_{\mu\nu}$, $B_{\mu\nu}$

are the field strength tensors for gluon, SU(2) and U(1), λ_a are 3×3 Gell-Mann matrices, $\vec{\tau}$ are the Pauli spin matrices, $Y = 1/3$ is weak hypercharge, g_s, g, g' are gauge coupling constants, f_s, f and f' are free parameters that are chosen equal to 1. η_{L} and η_{R} are the left-handed and the right-handed chirality factors, respectively. The couplings $\eta_{\mathrm{L/R}}$ are uniquely defined by the gauge-group representation of the excited states: η_{L} is only possible if the right-handed excited quarks are isospin doublets, while η_{R} is only possible if the left-handed excited quarks are isospin singlets. The normalization of the coupling was chosen such that $\max(|\eta_{\mathrm{L}}|, |\eta_{\mathrm{R}}|) = 1$ and chirality conservation requires $\eta_{\mathrm{L}}\eta_{\mathrm{R}} = 0$ [49].

We implemented this interaction Lagrangian into CalcHEP software [68] by using LanHEP [69, 70]. As we earlier mentioned in Section 1, there are four decay channels for q^* and in Fig. 2, we plotted total decay width with respect to the excited quark mass by taking compositeness scale equal to q^* mass and $\Lambda = 30$ TeV. It is illustrated that excited quark mass values positively correlated with decay widths.

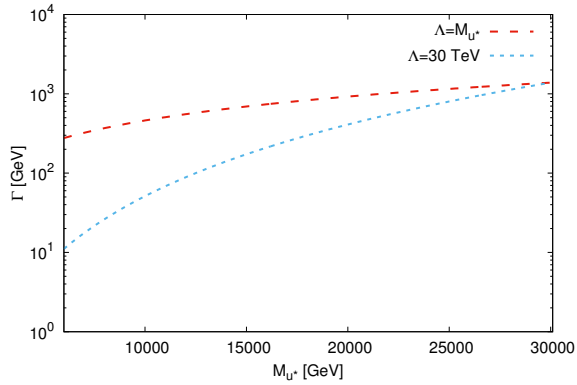

Fig. 2. u^* decay width correlations with excited quark mass at u^* mass equals compositeness scale and $\Lambda = 30$ TeV.

4. Excited u-quark production via proton collisions with unpolarized and polarized photon at $\sqrt{s}_{\gamma p} = 9.1$ and 28.8 TeV

In our calculation, we used two types of particle beams — proton and photon (see Section 2). 50 TeV proton beam comes from the FCC and we chose CTEQ6L quark distribution function [71, 72] with factorization and renormalization scales equal to M_{u^*} in numerical calculations. On the other hand, we had polarized and unpolarized high-energy photon beams [73, 74], which were obtained from the Compton backscattering [65–67] of laser beam on ILC or PWFA-LC electrons. The Feynman diagram for resonant production of u^* in photon–proton collisions is presented in Fig. 3.

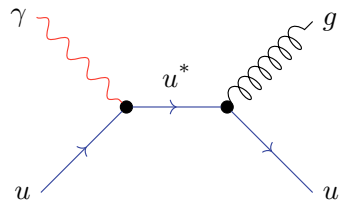

Fig. 3. Feynman diagram for signal.

4.1. Cross sections

In numerical calculations, we chose $\eta_{\rm L} = 1$, $\eta_{\rm R} = 0$ option for interaction Lagrangian (Eq. (1)). Following, we inserted corresponding electron and proton energies and chose laser photon option which corresponds to Compton backscattering photons in CalcHEP framework. The energy spectrum of backscattered laser photons we used is given in Refs. [65–67, 75] with a detailed explanation.

Figure 4 shows the cross-section values with respect to u^* mass for polarized (helicity $\gamma_{\mathcal{H}}$ equals 1 and -1) and unpolarized ($\gamma_{\mathcal{H}} = 0$) photon beams colliding with proton beam at 9.1 TeV center-of-mass energy. It is seen that excited quark could be produced with sufficiently high cross section up to roughly 8 TeV both for $\Lambda = 10$ TeV and $\Lambda = M_{u^*}$, corresponding to 10 events for 100 fb^{-1} luminosity value.

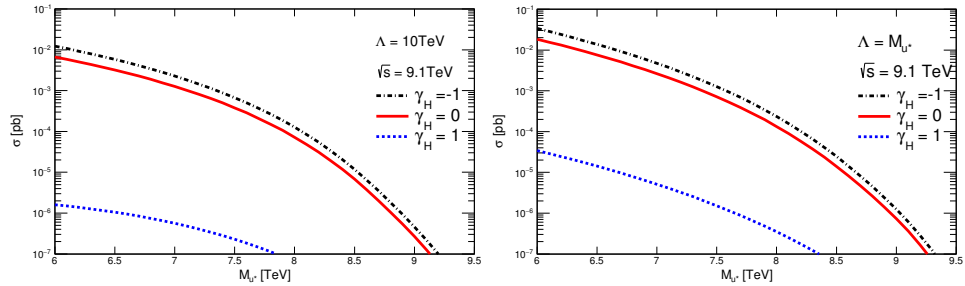

Fig. 4. u^* cross-section values with respect to its mass for proton collision with both polarized and unpolarized photon beams at $\sqrt{s} = 9.1$ TeV. On the left panel, compositeness scale was chosen as 10 TeV and on the right panel, u^* mass was taken the same as compositeness scale.

Figure 5 represents the same plots as the previous ones but this time, the center-of-mass energy is 28.8 TeV. It is seen that excited quark production could be achieved at higher mass values than previous collider option due to high center-of-mass energy in this collider option.

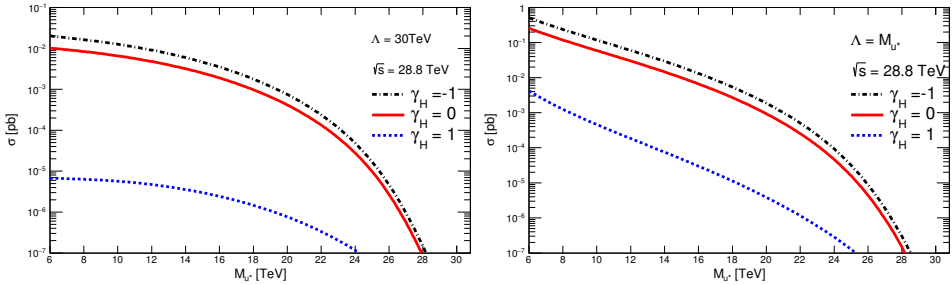

Fig. 5. u^* cross-section values with respect to its mass for proton collision with both polarized and unpolarized photon beams at $\sqrt{s} = 28.8$ TeV. On the left plot, compositeness scale was chosen as 30 TeV and on the right plot, u^* mass was taken the same as compositeness scale.

4.2. Signal and background analysis

4.2.1. Final-state distributions and cut determination

Our signal process is $\gamma + p \to u^* + X \to u + g + X$, therefore, background processes are represented by $\gamma + p \to j + j + X$, where j denotes u, $\bar{u}$, d, $\bar{d}$, c, $\bar{c}$, s, $\bar{s}$, b, $\bar{b}$ and g jets. To assign cuts for identifying the signal from background, we examined at the both signal and background transverse momentum (P_{T}), the pseudo-rapidity (η) and the invariant mass distributions for the final-state particles. Below, we present results for $\gamma_{\mathcal{H}} = -1$ case which corresponds to maximal signal cross-section values. It should be noted that we normalized cross-section values to plot P_{T} and η distributions for obtaining the cuts.

P_{T} distributions of the signal are the same for the two final-state particles (u, g) and the background P_{T} distributions' final-state particles that are jets, defined above. Figure 6 demonstrates P_{T} distributions of the signal and the background final-state jets for both two center-of-mass energy options. As expected for a single resonance, the usual Jacobean peaks appear for all mass values (6, 7, 10 and 15 TeV) of the signal. It is seen that when the applied P_{T} cut was taken 500 GeV for $\sqrt{s} = 9.1$ TeV and 1000 GeV for $\sqrt{s} = 28.8$ TeV, the background was reduced almost completely but the signal was remained nearly unchanged.

When the colliding beams have different energies, asymmetry occurs in signal and background distributions. So, we extracted η cuts using signal and background final-state jet distributions at their crossing point of their right-hand side limits, that are shown for both center-of-mass energies in Fig. 7. η distributions are presented as a sum of both final-state particles contributions because it is hard to identify gluon and u quark apart. On the other hand, we applied η cuts as -5.2 for the left-hand side of the η distributions, this value was taken from the CMS experiment forward subdetector limits [76]. We summarized all η cuts in Table II.

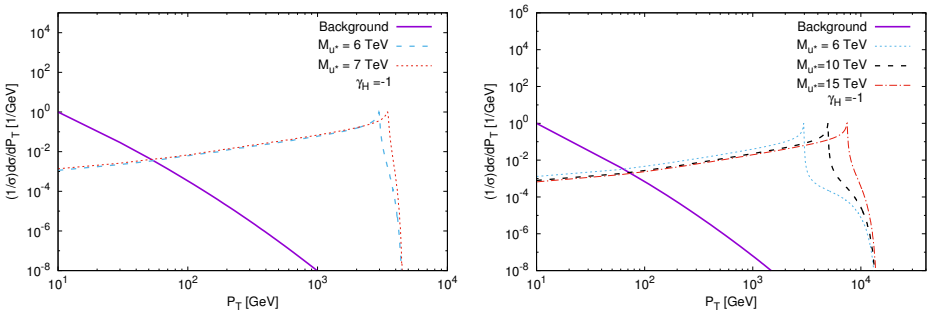

Fig. 6. Normalized P_{T} distributions of background and signal processes for $\sqrt{s} =$ 9.1 TeV (left panel) and for $\sqrt{s} = 28.8$ TeV (right panel).

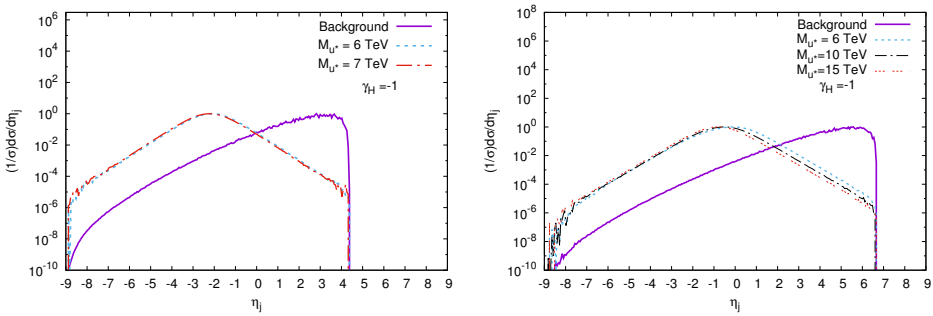

Fig. 7. Normalized η distributions of background and signal processes for $\sqrt{s} =$ 9.1 TeV (left panel) and for $\sqrt{s} = 28.8$ TeV (right panel).

TABLE II

List of the pseudo-rapidity cut limits for both the center-of-mass energy options.

$\sqrt{s}$ [TeV]	9.1				28.8			
$\gamma_{\mathcal{H}}$	-1		0		-1		0	
Cut limits	Min	Max	Min	Max	Min	Max	Min	Max
η_j	-5.2	0.0	-5.2	-0.2	-5.2	2.1	-5.2	2.0

Invariant mass distributions for signal and background processes are presented in Fig. 8. It is seen that signal peak values are above the background, so we determined invariant mass cut as $M_{u^*} - 2\Gamma_{u^*}$ and $M_{u^*} + 2\Gamma_{u^*}$ mass window, where M_{u^*} is u^* mass and Γ_{u^*} is the decay widths of the u^*.

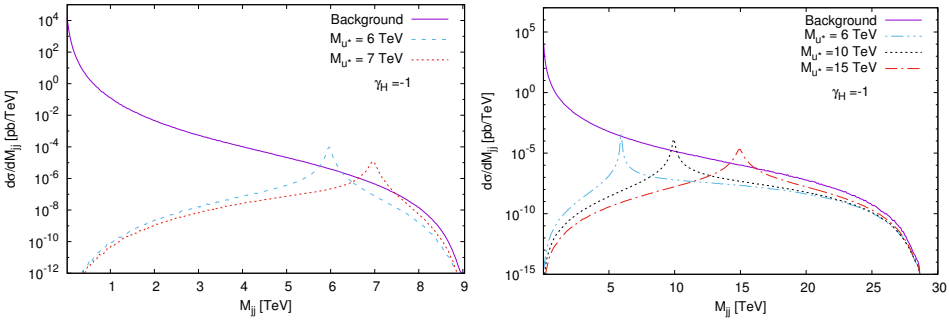

Fig. 8. Signal and background invariant mass distributions for $\sqrt{s} = 9.1$ TeV (left panel) and $\sqrt{s} = 28.8$ TeV (right panel) with $\gamma_{\mathcal{H}} = -1$.

4.2.2. Mass limits dependence on integrated luminosity and photon beam polarization

To extract the signal from the background, we used the cuts that were determined by distribution plots in the previous subsection. After that, Eq. (2) was utilized to calculate the statistical significance

$$S = \frac{\sigma_{\mathrm{S}}}{\sqrt{\sigma_{\mathrm{S}} + \sigma_{\mathrm{B}}}} \sqrt{\mathcal{L}_{\mathrm{int}}}\,, \tag{2}$$

where σ_{S} and σ_{B} are the signal and background cross-section values, respectively, and $\mathcal{L}_{\mathrm{int}}$ is the integrated luminosity. Obtained u^* mass limits were listed in Tables III and IV for both center-of-mass energies 9.1 TeV and 28.8 TeV colliders, respectively. According to Table I, integrated luminosity values are 10–100 fb^{-1} for ILC⊗FCC and 1–10 fb^{-1} for PWFA-LC⊗FCC options. As expected, higher integrated luminosity increased mass limits for u^*. Besides, it can be seen from Tables III and IV that photon beam

TABLE III

Excited u quark mass limits for 9.1 TeV center-of-mass energy γp collider.

$\sqrt{s}$		9.1 TeV							
$\mathcal{L}_{\mathrm{int}}$		10 fb^{-1}				100 fb^{-1}			
Λ		10 TeV		M_{u^*}		10 TeV		M_{u^*}	
$\gamma_{\mathcal{H}}$		-1	0	-1	0	-1	0	-1	0
Mass limits [TeV]	5σ	6.97	6.58	7.27	6.96	7.82	7.60	7.99	7.78
	3σ	7.41	7.11	7.62	7.37	8.08	7.90	8.23	8.05
	2σ	7.68	7.43	7.86	7.64	8.24	8.10	8.40	8.24

polarization enhanced u^* mass limits 0.21 TeV for 9.1 TeV CM and approximately 1.5 TeV for 28.8 TeV CM at their upper luminosity values if compared to unpolarized photon beam–proton collisions. In addition, the attainable best u^* mass limits could be achieved when the $\Lambda = M_{u^*}$.

TABLE IV

Excited u quark mass limits for 28.8 TeV center-of-mass energy γp collider.

$\sqrt{s}$		28.8 TeV							
$\mathcal{L}_{\text{int}}$		1 fb^{-1}				10 fb^{-1}			
Λ		15 TeV		M_{u^*}		30 TeV		M_{u^*}	
$\gamma_{\mathcal{H}}$		-1	0	-1	0	-1	0	-1	0
Mass limits [TeV]	5σ	13.8	8.94	14.2	12.1	17.1	14.5	19.4	17.9
	3σ	17.4	14.9	16.8	14.9	19.7	17.9	21.1	19.9
	2σ	19.5	17.6	18.5	16.9	21.3	19.8	22.2	21.2

In Fig. 9, we scanned luminosity values needed for the discovery (5σ), observation (3σ) and exclusion (2σ) of u^* as a function of its mass. It is seen that photon beam polarization enhanced attainable mass limits of u^*.

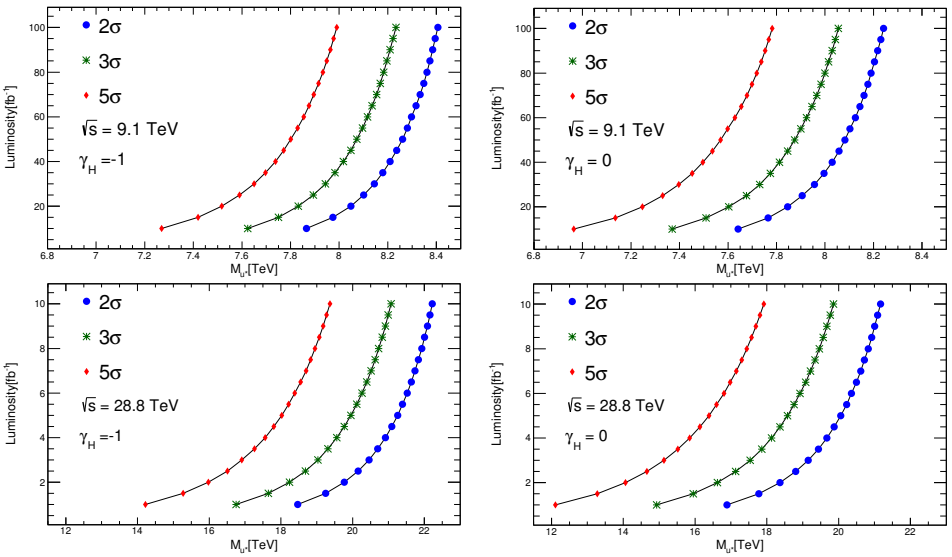

Fig. 9. The first row represents luminosity and u^* mass relations for $\sqrt{s} = 9.1$ TeV and the second row shows the same relations for $\sqrt{s} = 28.8$ TeV with $\Lambda = M_{u^*}$ at three different significance values. The left column corresponds to $\gamma_{\mathcal{H}} = -1$ and the right panel corresponds to $\gamma_{\mathcal{H}} = 0$.

4.2.3. Attainable compositeness scale

We took compositeness scale equal to u^* mass or some specific values as 10, 15 and 30 TeV until this subsection. At this point, we scanned both the compositeness scale values and u^* mass for discovery (5σ), observation (3σ), and exclusion (2σ) mass limits. It can be clearly noticed from Figs. 10 and 11 that the higher compositeness scales correspond to the lower u^* mass values. As it was expected, when the center-of-mass energy reached the 28.8 TeV with the highest luminosity value, the compositeness scale values had risen to the highest level for all u^* mass spectra. Furthermore, the photon beam polarization will afford an opportunity to probe bigger compositeness scale values than the unpolarized photon beam-proton collision.

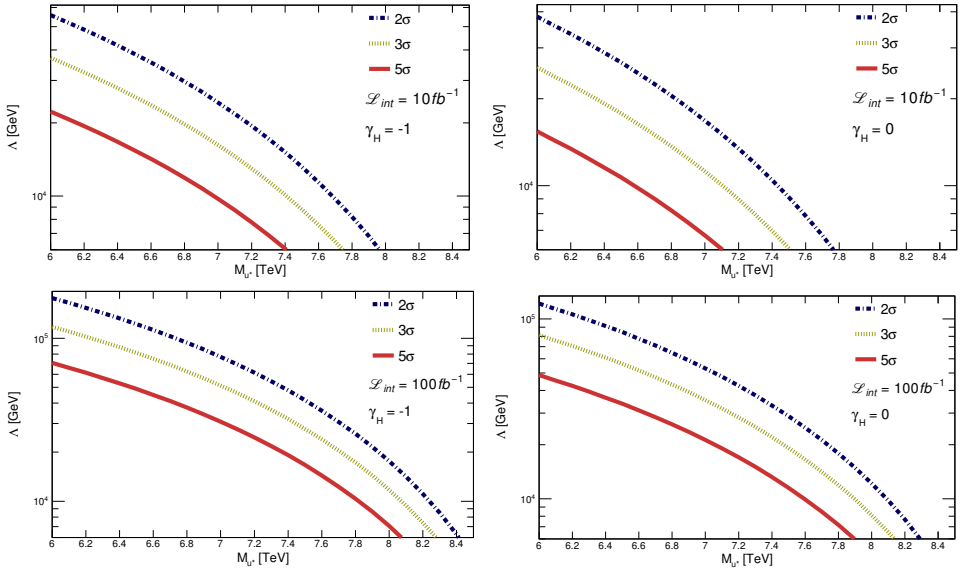

Fig. 10. The first row represents attainable Λ dependence on M_{u^*} for $\mathcal{L}_{\text{int}} = 10$ fb^{-1} and $\sqrt{s} = 9.1$ TeV. The second row shows the same relations for the same center-of-mass energy and $\mathcal{L}_{\text{int}} = 100$ fb^{-1}.

In Tables V and VI, we summarize the highest attainable compositeness scale quantities for various M_{u^*} values at the highest integrated luminosity values for both γp collider options. It is clearly seen that when the photon beam polarization is in charge, compositeness scale values increase for the whole M_{u^*} values. To illustrate, when we checked the compositeness scale values for $\sqrt{s} = 9.1$ TeV collider option with $M_{u^*} = 6$ TeV, the Λ value increased to 70.5 TeV from 48.7 TeV at the 5σ significance. Similarly, the compositeness scale value rose to 77.9 TeV from 51.9 TeV for $\sqrt{s} = 28.8$ TeV collider option with the same u^* mass values at the 5σ significance.

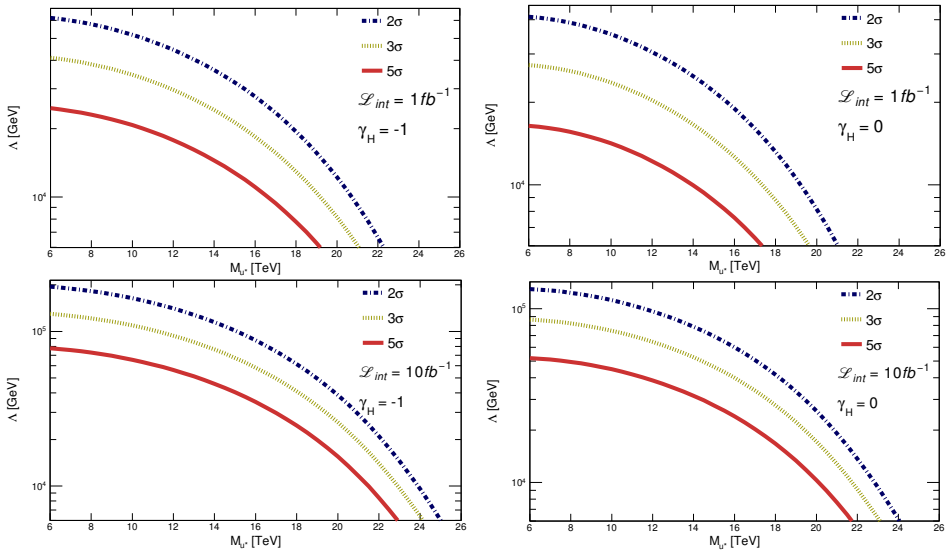

Fig. 11. The first row represents attainable Λ dependence on M_{u^*} for $\mathcal{L}_{\text{int}} = 1$ fb^{-1} and $\sqrt{s} = 28.8$ TeV. The second row shows the same relations for the same center-of-mass energy and $\mathcal{L}_{\text{int}} = 10$ fb^{-1}.

TABLE V

Attainable top Λ limits for M_{u^*} with the $\mathcal{L}_{\text{int}} = 100$ fb^{-1}.

CM [TeV]		9.1			
$\gamma_{\mathcal{H}}$		-1		0	
M_{u^*} [TeV]		6	7	6	7
Λ [TeV]	5σ	70.5	30.8	48.7	21.2
	3σ	117	51.3	81.2	35.4
	2σ	176	76.9	122	53.1

TABLE VI

Attainable top Λ limits for M_{u^*} with the $\mathcal{L}_{\text{int}} = 10$ fb^{-1}.

CM [TeV]		28.8					
$\gamma_{\mathcal{H}}$		-1			0		
M_{u^*} [TeV]		6	10	15	6	10	15
Λ [TeV]	5σ	77.9	65.6	40.5	51.9	44.8	27.7
	3σ	130	109	67.4	86.5	74.7	46.2
	2σ	195	164	101	130	112	69.4

4.2.4. Determination of the chirality structure of the q^*–q–γ vertex

The FCC-pp collider option will afford an opportunity to investigate M_{u^*} up to 50 TeV mass limit [77] which essentially exceeds potential capacity of γp collider options. However, the q^*–q–γ vertex could not be determined because the proton beams are unpolarized. The FCC-based γp colliders have capability of handling a polarized photon beam which will allow to determine chirality structure of the excited quark interactions. Afterward, we executed asymmetry calculations taking compositeness scales equal to u^* mass for $\eta_{\mathrm{L}} = 1$, $\eta_{\mathrm{R}} = 0$ and $\eta_{\mathrm{L}} = 0$, $\eta_{\mathrm{R}} = 1$ choices (η_{L} and η_{R} are chirality factors in Eq. (1)). Chirality structure of the q^*–q–γ vertex are distinguished by looking at the asymmetry numbers given in Table VII. Asymmetry calculation is done by Eq. (3)

$$\mathcal{A} = \frac{\sigma(\gamma_{\mathcal{H}} = 1) - \sigma(\gamma_{\mathcal{H}} = -1)}{\sigma(\gamma_{\mathcal{H}} = 1) + \sigma(\gamma_{\mathcal{H}} = -1)}, \tag{3}$$

where $\mathcal{A}$ denotes asymmetry, $\sigma(\gamma_{\mathcal{H}} = -1)$ corresponds to the cross-section numbers with helicity equal to -1 and $\sigma(\gamma_{\mathcal{H}} = 1)$ represents to cross-section numbers with helicity equal to 1.

TABLE VII

The polarization asymmetry for the excited u quark.

CM [TeV]	M_{u^*} [TeV]	$\gamma_{\mathcal{H}}$	$\eta_{\mathrm{L}} = 1,\ \eta_{\mathrm{R}} = 0$		$\eta_{\mathrm{L}} = 0,\ \eta_{\mathrm{R}} = 1$	
			σ [pb]	$\mathcal{A}$	σ [pb]	$\mathcal{A}$
9.1	6	-1	4.15×10^{-2}	-0.99	8.07×10^{-5}	0.99
		1	1.71×10^{-4}		2.29×10^{-2}	
	7	-1	6.50×10^{-3}	-0.98	2.78×10^{-5}	0.98
		1	5.89×10^{-5}		3.54×10^{-3}	
28.8	10	-1	1.39×10^{-1}	-0.99	4.34×10^{-4}	0.99
		1	9.20×10^{-4}		7.61×10^{-2}	
	15	-1	2.23×10^{-2}	-0.99	3.56×10^{-5}	0.99
		1	7.54×10^{-5}		1.23×10^{-2}	

5. Conclusion

In this work, we analyzed resonance production of the excited u quark at the FCC-based γp colliders that offer two possibilities: $\sqrt{s}_{\gamma p}^{\max} = 9.1$ TeV with $\mathcal{L}_{\rm int} = 10$–$100$ fb^{-1} (ILC$\otimes$FCC) and $\sqrt{s}_{\gamma p}^{\max} = 28.8$ TeV with $\mathcal{L}_{\rm int} = 1$–$10$ fb^{-1} (PWFA-LC$\otimes$FCC). It should be noted that at this stage, we did not consider hadronization and detector effects which may lead to some decrease of discovery limits on u^* mass and compositeness scale.

We conducted calculation of the u^* mass limits for discovery (5σ), observation (3σ) and exclusion (2σ) confidence levels at the 10, 15, 30 TeV compositeness scales and at $\Lambda = M_{u^*}$, but the highest mass limits are achieved by taking M_{u^*} equal to Λ. As seen from Tables III and IV, the photon beam polarization increases the mass limits for all confidence levels. For $\gamma_{\mathcal{H}} = -1$, $\Lambda = M_{u^*}$ and $\mathcal{L}_{\rm int} = 100$ fb^{-1}, attainable mass limits are 7.99 TeV for 5σ, 8.23 TeV for 3σ and 8.40 TeV for 2σ at $\sqrt{s} = 9.1$ TeV collider option. Concerning the highest center-of-mass energy collider option ($\sqrt{s} = 28.8$ TeV), the biggest attainable mass limits become 19.4 TeV for 5σ, 21.1 TeV for 3σ and 22.2 TeV for 2σ confidence levels. To address these findings, ATLAS and the CMS excluded M_{u^*} up to 6 TeV with 37 fb^{-1} integrated luminosity at $\sqrt{s} = 13$ TeV (with $\sqrt{s} = 14$ TeV and $\mathcal{L}_{\rm int} = 300$ fb^{-1}, this limit will potentially increase to $M_{u^*} = 7.5$ TeV). Therefore, the FCC-γp collider essentially superiors (3 times) the LHC potential.

Besides the specific values of the compositeness scale, we scanned the compositeness scale with respect to M_{u^*}. Our calculation results show that the highest compositeness scale value is provided by the photon beam polarization (see Tables V and VI). Compositeness scale values are evaluated as 77.9 TeV for 5σ, 130 TeV for 3σ and 195 TeV for 2σ at the $\sqrt{s} = 28.8$ TeV with $\mathcal{L}_{\rm int} = 10$ fb^{-1}, $M_{u^*} = 6$ TeV and $\gamma_{\mathcal{H}} = -1$. These values essentially exceed the LHC potential but the FCC-pp is much higher [77].

Finally, if the excited quarks mass lies in the region mentioned above, the FCC-pp collider will apparently discover u^* before the construction of FCC-based γp colliders. However, as seen from this study, the latter ones will provide a unique opportunity to determine chirality structure of u^*–u–γ vertex by using the polarized photon beam.

This study is supported by TUBITAK under the grant No. 114F337. We thank Professor Yasar Onel for his support and contribution for encouraging such a research.

REFERENCES

[1] S. Chatrchyan *et al.*, *Phys. Lett. B* **716**, 30 (2012).

[2] G. Aad *et al.*, *Phys. Lett. B* **716**, 1 (2012).

[3] J.C. Pati, A. Salam, *Phys. Rev. D* **10**, 275 (1974) [*Erratum ibid.* **11**, 703 (1975)].

[4] I.A. D'Souza, C.S. Kalman, *Preons: Models of Leptons, Quarks and Gauge Bosons as Composite Objects*, World Scientific, 1992.

[5] M.A. Shupe, *Phys. Lett. B* **86**, 87 (1979).

[6] H. Harari, *Phys. Lett. B* **86**, 83 (1979).

[7] H. Terazawa, *Phys. Rev. D* **22**, 184 (1980).

[8] H. Terazawa, M. Yasuè, K. Akama, M. Hayashi, *Phys. Lett. B* **112**, 387 (1982).

[9] H. Terazawa, *Phys. Lett. B* **133**, 57 (1983).

[10] E.J. Eichten, K.D. Lane, M.E. Peskin, *Phys. Rev. Lett.* **50**, 811 (1983).

[11] H. Fritzsch, G. Mandelbaum, *Phys. Lett. B* **102**, 319 (1981).

[12] A. Çelikel, M. Kantar, S. Sultansoy, *Phys. Lett. B* **443**, 359 (1998).

[13] M.E. De Souza, *Scientia Plena* **4**, 6 (2008).

[14] H. Fritzsch, *Mod. Phys. Lett. A* **31**, 1630019 (2016).

[15] F.E. Low, *Phys. Rev. Lett.* **14**, 238 (1965).

[16] F.M. Renard, *Il Nuovo Cim. A* **77**, 1 (1983).

[17] J. Kühn, P. Zerwas, *Phys. Lett. B* **147**, 189 (1984).

[18] G. Pancheri, Y.N. Srivastava, *Phys. Lett. B* **146**, 87 (1984).

[19] A. De Rújula, L. Maiani, R. Petronzio, *Phys. Lett. B* **140**, 253 (1984).

[20] K. Hagiwara, S. Komamiya, D. Zeppenfeld, *Zeit. Phys. C* **29**, 115 (1985).

[21] J.H. Kühn, H.D. Tholl, P.M. Zerwas, *Phys. Lett. B* **158**, 270 (1985).

[22] U. Baur, I. Hinchliffe, D. Zeppenfeld, *Int. J. Mod. Phys. A* **2**, 1285 (1987).

[23] M. Spira, P.M. Zerwas, *Excited Quarks and Leptons* in: *Heavy Flavours and High-Energy Collisions in the 1–100 TeV Range*, Springer, 1989, pp. 519–529.

[24] U. Baur, M. Spira, P.M. Zerwas, *Phys. Rev. D* **42**, 815 (1990).

[25] F. Boudjema, A. Djouadi, J.L. Kneur, *Zeit. Phys. C* **57**, 425 (1993).

[26] O. Çakır, R. Mehdiyev, *Phys. Rev. D* **60**, 034004 (1999).

[27] O. Çakır, C. Leroy, R. Mehdiyev, *Phys. Rev. D* **62**, 114018 (2000).

[28] O. Çakır, C. Leroy, R. Mehdiyev, *Phys. Rev. D* **63**, 094014 (2001).

[29] O.J.P. Éboli, S.M. Lietti, P. Mathews, *Phys. Rev. D* **65**, 075003 (2002).

[30] O. Çakır, A. Yılmaz, S. Sultansoy, *Phys. Rev. D* **70**, 075011 (2004).

[31] O. Çakır, C. Leroy, R. Mehdiyev, A. Belyaev, *Eur. Phys. J. C* **32**, 1 (2004).

[32] O. Çakır, A. Ozansoy, *Phys. Rev. D* **77**, 035002 (2008).

[33] A. Caliskan, S.O. Kara, A. Ozansoy, *Adv. High Energy Phys.* **2017**, 1540243 (2017).

[34] A. Caliskan, *Adv. High Energy Phys.* **2017**, 4726050 (2017).

[35] F. Abe *et al.*, *Phys. Rev. Lett.* **74**, 3538 (1995).

[36] C. Adloff *et al.*, *Eur. Phys. J. C* **17**, 567 (2000).

[37] M. Acciarri *et al.*, *Phys. Lett. B* **502**, 37 (2001).

[38] S. Chekanov *et al.*, *Phys. Lett. B* **549**, 32 (2002).

[39] J. Abdallah *et al.*, *Eur. Phys. J. C* **46**, 277 (2006).

[40] V. Khachatryan *et al.*, *Phys. Lett. B* **738**, 274 (2014).

[41] G. Aad *et al.*, *J. High Energy Phys.* **2016**, 41 (2016).

[42] G. Aad *et al.*, *Phys. Lett. B* **754**, 302 (2016).

[43] M. Aaboud *et al.*, Search for New Phenomena in Dijet Events Using 37 fb^{-1} of pp Collision Data Collected at $\sqrt{s}$ =13 TeV with the ATLAS Detector, Technical Report, 2017.

[44] V. Khachatryan *et al.*, *Phys. Rev. Lett.* **116**, 071801 (2016).

[45] CMS Collaboration, Excited Quarks in the Photon+Jet Final State in Proton–Proton Collisions at $\sqrt{s} = 13$ TeV, Technical Report CMS-PAS-EXO-16-015, CERN, Geneva 2016.

[46] A.M. Sirunyan *et al.*, *Phys. Lett. B* **769**, 520 (2017).

[47] CMS Collaboration, Search for Excited States of Light and Heavy Flavor Quarks in the γ+jet Final State in Proton–Proton Collisions at $\sqrt{s} = 13$ TeV, Technical Report CMS-PAS-EXO-17-002, CERN, Geneva 2017.

[48] M. Sahin, S. Sultansoy, S. Turkoz, *Phys. Rev. D* **83**, 054022 (2011).

[49] C. Patrignani *et al.*, *Chin. Phys. C* **40**, 100001 (2016).

[50] Y.C. Acar *et al.*, *Nucl. Instrum. Methods Phys. Res. A* **871**, 47 (2017).

[51] Future Circular Collider Study Kickoff Meeting, University of Geneva, February 12–15, 2014, `http://indico.cern.ch/e/fcc-kickoff`

[52] A.K. Çiftçi, S. Sultansoy, Ş. Türköz, Ö. Yavaş, *Nucl. Instrum. Methods Phys. Res. A* **365**, 317 (1995).

[53] S. Sultanov, Prospects of the Future ep and γp Colliders: Luminosity and Physics, Technical Report, International Centre for Theoretical Physics, 1989.

[54] B.H. Wiik, *Recent Development in Accelerators*, Proc. of the Int. Europhysics Conference on High Energy Physics, Marseille, France, July 1993, pp. 739–758.

[55] R. Brinkmann *et al.*, `arXiv:physics/9712023 [physics.acc-ph]`.

[56] S. Sultansoy, *Turkish J. Phys.* **22**, 575 (1998).

[57] S. Sultansoy, The PostHERA Era: Brief Review of Future Lepton Hadron and Photon Hadron Colliders, DESY-99-159, AU-HEP-99-02, 1999.

[58] S. Sultansoy, *Eur. Phys. J. C* **33**, 1064 (2004).

[59] A.N. Akay, H. Karadeniz, S. Sultansoy, *Int. J. Mod. Phys. A* **25**, 4589 (2010).

[60] J.L. Abelleira Fernandez *et al.*, *J. Phys. G* **39**, 075001 (2012).

[61] M. Benedikt, F. Zimmermann, Future Circular Colliders, Technical Report, FCC-DRAFT-ACC-2015-032, 2015.

[62] J. Wenninger, M. Benedikt, K. Oide, F. Zimmermann, Future Circular Collider Study Lepton Collider Parameters, CERN EDMS No. 1346082, 2014.

[63] J. Wenninger *et al.*, Future Circular Collider Study Hadron Collider Parameters, Technical Report FCC-1401201640-DSC, 2014.

[64] H. Aksakal *et al.*, *Nucl. Instrum. Methods Phys. Res. A* **576**, 287 (2007).

[65] I.F. Ginzburg, G.L. Kotkin, V.G. Serbo, V.I. Telnov, *Nucl. Instrum. Methods Phys. Res.* **205**, 47 (1983).

[66] I.F. Ginzburg *et al.*, *Nucl. Instrum. Methods Phys. Res.* **219**, 5 (1984).

[67] V.I. Telnov, *Nucl. Instrum. Methods Phys. Res. A* **294**, 72 (1990).

[68] A. Belyaev, N.D. Christensen, A. Pukhov, *Comput. Phys. Commun.* **184**, 1729 (2013).

[69] A.V. Semenov, LanHEP: A Package for Automatic Generation of Feynman Rules in Field Theory, Version 2.0, 2002.

[70] A. Semenov, *Comput. Phys. Commun.* **201**, 167 (2016).

[71] J. Pumplin *et al.*, *J. High Energy Phys.* **0207**, 012 (2002).

[72] D. Stump *et al.*, *J. High Energy Phys.* **0310**, 046 (2003).

[73] D.L. Borden, D.A. Bauer, D.O. Caldwell, *Phys. Rev. D* **48**, 4018 (1993).

[74] A. D'Angelo *et al.*, *Nucl. Instrum. Methods Phys. Res. A* **455**, 1 (2000).

[75] A. Pukhov, A. Belyaev, N. Christensen, CalcHEP — Calculator for High Energy Physics — A Package for Evaluation of Feynman Diagrams, Integration Over Multi-particle Phase Space, and Event Generation, CalcHEP Manual 3.3.6 edition, July 2012.

[76] V. Khachatryan *et al.*, *Phys. Rev. C* **92**, 034911 (2015).

[77] A.N. Akay, Y.O. Günaydin, M. Sahin, S. Sultansoy, in preparation.